Numerical study of a ventilated ceiling that integrates a phase change material for design improvement

Wael Zeitoun, Matthieu Labat, Sylvie Lorente, Matthieu Cezard

Numerical study of a ventilated ceiling that integrates a Phase Change Material for design improvement

Wael Zeitoun[1], Matthieu Labat[1*], Sylvie Lorente[2], Matthieu Cézard[1]

[1]LMDC, INSA/UPS Génie Civil, 135 Avenue de Rangueil, 31077 Toulouse cedex 04 France.
[2]Villanova University, Department of Mechanical Engineering, Villanova, PA 19085, USA

*Corresponding author: m_labat@insa-toulouse.fr

Abstract

Thermally Activated Building Systems (TABS) are building elements that transfer and sometimes store thermal energy. By embedding the fluid network into a massive layer, TABS can effectively reduce indoor temperature variation and cooling demand. However, their application is limited to new constructions, and there is a need to adapt this concept for refurbishment. One solution to improve cooling efficiency is to use Phase Change Materials (PCM). These materials rely on latent heat for phase change instead of sensible heat only. In this paper, a suspended ceiling that supports PCM modules is considered, with air circulating between the PCM and an existing concrete slab. Heat transfer at different stages was modelled, progressively increasing the complexity of the system. The results demonstrate that the melting temperature should be between 15 to 17°C for effective cooling. The need for an additional thermal resistance between the PCM and the room was highlighted, as it has been discovered that it plays a crucial role in the thermal behaviour of the entire system and can promote energy storage when it reaches a certain level. Conversely, lower values should be chosen if a radiative heat flux through the ceiling is desired.

Keywords

Thermally Activated Building Systems, Phase Change Materials, Suspended Radiant Ceiling, Heat and mass transfer, Numerical simulation

Nomenclature

Latin Symbols	Description	Unit
A	Cross section of the channel	m^2
a	Dimension	m
b	Dimension	m
C_p	Specific heat capacity	$J.kg^{-1}.K^{-1}$
d	Thickness	m
E	Energy	kWh
F	Fraction of heat flow	-
h	Coefficient for heat transfer	$W.m^{-2}.K^{-1}$
k	Thermal conductivity	$W.m^{-1}.K^{-1}$
L	Length	m
L_f	Latent heat of fusion	$J.kg^{-1}$
L_m	Length for complete melting	m
$\dot{m}$	Mass flow rate	$kg.s^{-1}$
m_f	Local melting fraction	-
M_f	Global melting fraction	-
Nu	Nusselt number	-
P	Power	kW
p	Pressure	Pa
q_v	Volumetric flow rate	$m^3.s^{-1}$
R	Thermal resistance	$m^2.K.W^{-1}$
Re	Reynolds number	-
s	Position of the melting front in a 1D problem	m
SF	Step Function	-
T	Temperature	K
t	time	s
$\boldsymbol{u}$	Velocity vector	$m.s^{-1}$
u	Velocity component in x direction	$m.s^{-1}$
U	Average fluid velocity	$m.s^{-1}$
W	Width	m
x	Abscissa	m
y	Ordinate	m
Greek Symbols		
α	Thermal diffusivity	$m^2.s^{-1}$
θ	Dimensionless temperature	-
μ	Dynamic viscosity	Pa.s
ρ	Density	$kg.m^{-3}$
ϕ	Heat flow rate	W
Subscripts		
$_a$	air	
$_b$	blown	

$_{c}$	Channel, convective	
$_{Con}$	Concrete	
$_{in}$	Inlet, entering	
$_{ins}$	insulatioin	
$_{m}$	mean	
$_{max}$	maximum	
$_{min}$	minimum	
$_{Melt}$	Melting point	
$_{out}$	outlet	
$_{PCM}$	Phase change material	
$_{R}$	Released	
$_{r}$	room	
$_{T}$	Total, period	
$_{t}$	transmitted	
$_{tot}$	Total	
$_{w}$	wall	
$_{0}$	Referring to sensible specific heat capacity of the PCM	

1. Introduction

Building energy consumption currently represents around 40% of total energy consumption in Europe and Northern America. Therefore, significant research efforts have been made over the last few decades to limit and reduce this figure. Initially, research efforts focused on reducing the energy demand for heating, which is significant, and much remains to be done. However, it is also important to address the cooling demand in light of the potential impact of climate change towards the end of the century (Elnagar et al., 2023). While this impact may not be uniform, certain regions, such as southern Europe, may experience an increase in the cooling demand higher than 200% (Ciancio et al., 2020). This stresses the urge for adapting the building stock to hot outdoor conditions.

In the scientific literature, various technical solutions have been studied to reduce peak energy demand, especially those related to the thermal inertia of some building elements. (Di Perna et al., 2011) compared various multi-layer wall configurations with similar global performance but different arrangement and concluded that a massive layer close to the inner surface of the envelope effectively reduces the surface temperature in summer. (Kuczyński et al., 2021)

demonstrated that a high thermal mass can be effective when combined with night ventilation and proper use of external blinds. This highlights that thermal inertia of the envelope alone is not a solution to increasing cooling demand, and it explains the growing interest in Thermally Activated Building Systems (TABS). These are building elements that actively transfer and sometimes store thermal energy. Such elements include water pipes or air ducts that are embedded in the building surfaces or structure to operate as heat exchangers, transferring heat to the spaces of the building (Romaní et al., 2016). When embedding the fluid network into a massive layer, TABS can effectively trigger the thermal inertia of structural elements, mitigating indoor temperature variation and reducing cooling demand. Ceilings and floors are often used as massive TABS due to their large surface area exposed to the indoors, facilitating heat transfer with the controlled room.

To that extent, ceilings and floors contribution to indoor heat balance and user comfort can be compared to the use of radiant panels. The latter are known to improve indoor comfort by promoting radiant heat transfer compared to purely convective solutions (Rhee et al., 2017). The concept of massive heating floors has been extensively developed in China (Zhuang et al., 2009) and Korea (Yeo et al., 2003), using air as the medium to transport heat. It was later extended to cooling ceilings in the 1990s, taking advantage of the use of hollow core concrete as demonstrated in (Corgnati and Kindinis, 2007; Mohammad et al., 2014; Winwood et al., 1994; Zmeureanu and Fazio, 1988). Initially, the cores were used to reduce the weight of the slab and production costs. Subsequently, they were also used for air circulation, eliminating the need for suspended ceilings. Another type of cooling ceiling is the embedded air-duct system, also known as ventilated slab, which differs from hollow-core concrete as it is cast in-situ (Labat et al., 2021).

Although the basic concept of such systems is simple, a major issue in their adoption is related to control. The slow response time makes it difficult to maintain the indoor temperature within a narrow range under time-varying heat loads. However, this issue can be addressed by advanced controlling techniques, as exemplified in (Labat and Hazyuk, 2023; Park and Krarti, 2019). A further limitation arises from the use of embedded pipes, which must be selected and designed early in the construction of new buildings. For this reason, ventilated slabs cannot be easily integrated into existing buildings for retrofitting. However, retrofitting buildings is a major lever in adapting to climate change due to the slow turnover of the building stock. Therefore, there is a need to adapt the concept of massive cooling ceilings for refurbishment.

Promoting heat transfer with an existing slab is a challenging task because it cannot be modified to include a piping network in its core. An alternative option is to consider adding extra layers to the existing slab, allowing the media that transport heat to lie in between the ceiling and the layers. However, the mechanical properties of a slab are generally designed for a specific load, and it cannot bear an additional significant load. In other words, the issue is how to increase thermal inertia without altering the current slab or adding a heavy layer. One solution is to use Phase Change Materials (PCM), which rely on latent heat for phase change rather than sensible heat. This results in a higher energy storage density and a reduced mass that needs to be added.

PCM technology has reached maturity, and a wide variety of products are available on the market, making it possible to consider a large range of applications depending on the targeted temperature for phase change. The scientific literature has already comprehensively studied the use of PCM for saving energy in building applications (Soares et al., 2013). For instance, (Royon et al., 2014) used it to fill a hollow core slab, enhancing its thermal performance. In the context of refurbishment, ventilated slab solution where air is circulated between the existing

concrete slab and a suspended ceiling that contains PCM has also been studied. This configuration can be seen as a combination of an air-to-PCM heat exchanger and a Suspended Radiant Ceiling (SRC). Experimental results for various air-to-PCM heat exchanger configurations can be found in (Dallaire et al., 2022; Dolado et al., 2011; Labat et al., 2014; Lazaro et al., 2009; Stathopoulos et al., 2017). (Mousavi et al., 2021) reviewed 24 studies on suspended cooling ceilings that incorporate PCM. In most cases, a water piping network was used to cool and solidify the PCM. However, (Weinläder et al., 2014, 2013) used air instead, making their study a notable exception. To the best of the author's knowledge, (Weinläder et al., 2014) study is the closest to the concept presented here. Although the authors provide detailed and valuable experimental results obtained at the room scale, they do not discuss the design of the system, particularly with regard to the fundamentals of heat and mass transfer.

The aim of this paper is to contribute to the development of ventilated slabs in the context of refurbishment through a theoretical study that focuses on the design stage. As previously stated, similar systems are rather scarce in the literature, and a general methodology is lacking to identify the role of the different components in the kinetic of heat transfer and to provide an early sizing. For this reason, the methodology presented here will rely on simple numerical modelling of heat and mass transfer, especially when it comes to the modelling of phase change, in order to facilitate the analysis of the thermal performance of the system. Simplified material properties will be considered in order to avoid focusing on a specific product and remain general, so that the methodology provided here could be applied to various configurations to provide an early design. The selection of the final materials is beyond the scope of this study.

The system under consideration can be described as a suspended ceiling that supports PCM modules, with air circulating between the PCM and an existing concrete slab. In order to gain

insight into the influence of each parameter, the study will model the heat transfer at different stages, progressively increasing the complexity of the system.

1. The convective heat transfer coefficient will be determined by first modelling the air channel. Literature results will be used for validation purposes.
2. The study will focus solely on the system itself, without considering heat transfer with the surrounding room. This will facilitate the selection of the PCM. To avoid product specificity, the thermal behaviour of the PCM was modelled using simple mathematical functions. Heat transfer with the concrete slab will be included. The kinetics of heat transfer will be discussed, with particular attention paid to the evolution of the melting fraction within the PCM. This will be achieved by examining step and cyclic temperature variations at the inlet of the channel, assuming a constant airflow rate.
3. Finally, the modelling will include heat transfer with the room located below, assuming a constant temperature for the latter. The addition of a thermal resistive layer below the PCM will be considered and discussed. The analysis of results will consider the phases of solidification and melting separately. The model will allow for a breakdown of how the cooling power supplied to the system is distributed between the different elements during the solidification phase. With respect to the melting phase, the cooling power will be evaluated and compared with the results obtained experimentally for similar systems in the literature.

2. Design of the air channel

The initial constraint concerns the airflow rate q_v that will be introduced into the channel. This rate is dependent on the room and its intended use, as the French labour code mandates a minimum airflow rate. The purpose of the airflow rate is to eliminate or at least reduce

pollutants such as exhaled CO_2 and volatile organic compounds, and to ensure satisfactory air renewal rates for office workers. The hygienic airflow rate for office rooms is 25 $m^3.h^{-1}$ per person. Consequently, the minimum airflow rate is 50 $m^3.h^{-1}$. An upper limit of 150 $m^3.h^{-1}$ has also been proposed. The statement corresponds to the industrial estimation of when the system becomes economically less attractive than an all-air HVAC treatment. To achieve the global objective of providing and storing cooling power in the office, a higher airflow rate is preferable. For this reason, the maximum value of 150 $m^3.h^{-1}$ will be used for q_v for the remainder of this study. This paper focuses on a typical office room designed for two people and located in an existing office building in France. In France, office building interiors are typically defined using *trames*, which are facade lengths of around 1.35 m that can accommodate a window. It is recommended that the room width be two *trames*. The office room dimensions are as follows: the width W_r is 2.70 m, the depth L_r is 5 m, and the height H_r is 3 m. These values correspond to the inner distances and do not account for the thickness of walls, partitions, slabs, and the suspended system under study.

2.1. Theoretical elements

The ventilation channel aims to enhance heat transfer between the air and the solid walls. In other words, the goal is to achieve the highest value for convective heat transfer. The channel's geometry is a degree of freedom since the volumetric airflow rate is fixed. To simplify and enable rapid construction, a channel has been proposed in this paper. The air can be circulated from the corridor to the other side of the room near the windows by elevating panels parallel to the ceiling and creating a small channel, as depicted in Figure 1. A grid should be used at the inlet of the channel to ensure a uniform airflow rate throughout the width of the channel, allowing for a 2D model of the problem.

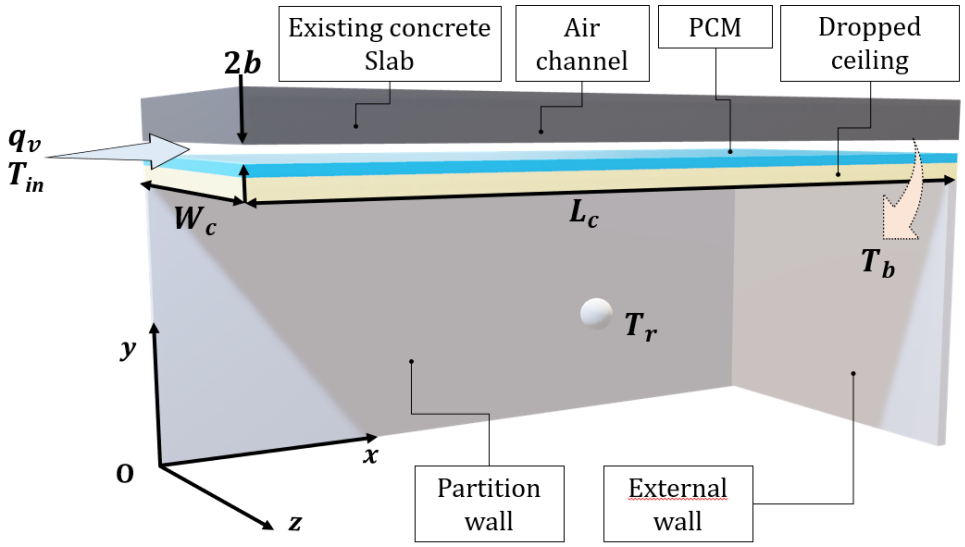

Figure 1 : Overview of the designed system.

The Reynolds number characterizes the flow regime within the channel and is defined by:

$$Re = \frac{\rho_a U L_c}{\mu_a} \tag{1}$$

The characteristic length of a rectangular duct L_c is given by:

$$L_c = \frac{4\,ab}{a+b} \tag{2}$$

Where a and b are the same dimensions as in Figure 2.

It is important to note that the use of a thin channel is subject to real estate and heat transfer considerations. Firstly, a smaller channel would occupy less space and be more easily accepted in the context of refurbishment. Secondly, a thin channel geometry leads to higher Nusselt numbers, which are desirable for heat transfer. This is easily observed for the laminar case in the classic reference (Shah et al., 1971) as shown in Figure 2, where case 3 is close to the actual channel configuration. Figure 2 was determined for some of the walls maintained at a constant temperature, the others being considered as adiabatic. PCM absorbs or releases heat at a specific temperature range. Although a temperature range differs from a constant value, it is

close to the theoretical case. As the design phase focuses on phase change to make the best use of the PCM, the assumption of a constant wall temperature is relevant.

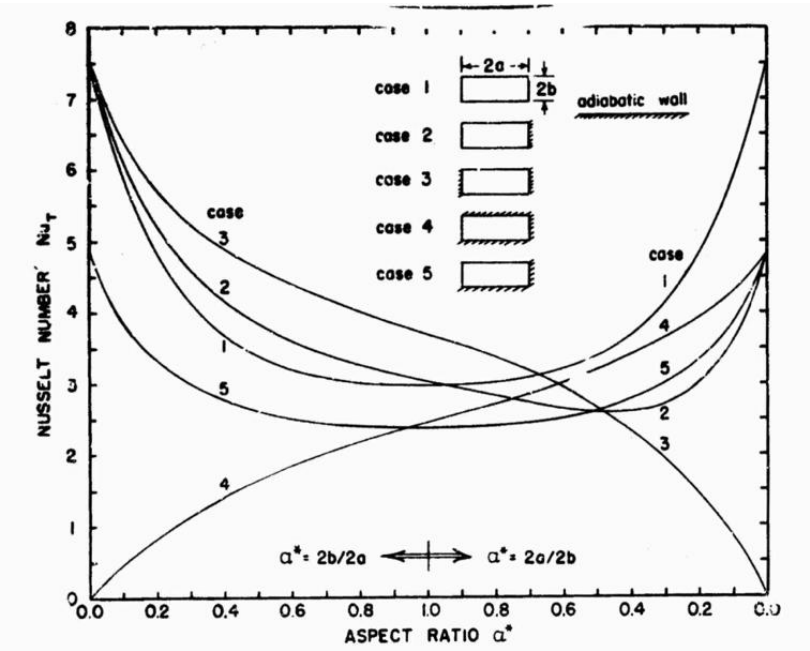

Figure 2 : Nusselt number for a forced laminar flow in a rectangular duct at constant wall temperature, where some of the walls are adiabatic (Shah et al., 1971).

The underlying assumption of laminar flow used to obtain the results in Figure 2 is discussed below. In this case of two parallel plates, the characteristic length is approximately twice the distance that separates them. By replacing L_c in equation (1) and introducing the volumetric flow rate q_v, it gives for this specific scenario:

$$Re = \frac{\rho_a \, 4 \, q_V}{\mu_a \, 4(a+b)} \approx \frac{2 \, \rho_a \, q_V}{\mu_a \, W_c} \qquad (3)$$

The equation demonstrates that the flow regime is very little dependent on b when the volumetric flow rate in the channel is fixed for a thin channel, and that it varies with the width of the channel W_c. To enhance heat transfer through convection and radiation from the ceiling, W_c should be increased to maximize the area that exchange with the room. Therefore, it should be equal to the width of the room, W_r. In this situation, the Reynolds number is near 2000, indicating a laminar flow. While a turbulent flow (Re $>$ 4000) could be achieved by reducing

the width of the channel, a wide channel is more desirable as previously mentioned and turbulent flow won't be considered in the rest of this study.

Regarding now the general definition of the Nusselt number Nu and Figure 2, it can be seen that a small variation of the channel thickness does not significantly affect the Nusselt number, which should be close to 7.5. However, the convective coefficient h_c is at its maximum in a thin channel. Therefore, to promote heat transfer, a thin and wide channel should be used. The value retained for d is 1 cm. It might be hard to achieve such a thin channel at the room scale in practice, yet not impossible. It is acknowledged however that larger values might be preferable for practical constraints. The next part of this chapter is dedicated to the validation of the numerical model thanks to the theoretical results obtained in (Shah et al., 1971).

2.2. Analytical validation of the modelling of heat transfer within the air channel

A commercial finite element software (COMSOL) was selected to model heat transfer in the air channel. This software is a general-purpose tool designed to solve partial differential equations. It includes a meshing tool that is adapted to 2D and 3D geometries. It has already been applied by others to the modelling of heat exchangers that include PCM, as exemplified in (Al-Saadi and Zhai, 2013; Bianco et al., 2022; Michel et al., 2017). It was used to compute heat balance in the air layer, which is given by:

$$W_c \, \rho_a C_{p,a} \left(\frac{\partial T}{\partial t} + \boldsymbol{u} \cdot \boldsymbol{\nabla} T \right) - \boldsymbol{\nabla} \cdot (W_c k_a \boldsymbol{\nabla} T) = 0 \qquad (4)$$

The Navier-Stokes equation can be used to model laminar flow. However, assuming a fully developed flow, the analytical solution is simple and can be used to reduce the computational time. Practitioners generally consider an upper limit of 5 $m.s^{-1}$, sometimes even decreased to 3 $m.s^{-1}$, as exceeding this limit may jeopardize the acoustic comfort of office workers. In the

present situation, the maximum velocity is approximately 2.3 m.s^{-1}, which complies with these recommendations.

As the problem exhibits a symmetry axis, only one half was modelled to decrease computational time, as shown in Figure 3. A steady-state simulation was used, where air was blown into the channel at a constant temperature, T_{in}, set at 12°C, while the wall temperature, T_w, was maintained at 24°C. During early studies, mesh sensitivity was assessed, and it was found that the results were highly dependent on the mesh refinement in the thickness of the air layer (y-axis), but less so in the direction of the flow (x-axis). A structured mesh defined with 30 elements in the thickness, including a boundary layer of 0.5 mm that contains 10 elements, produced stable results. A larger and regular mesh was used in the flow direction, as shown in Figure 3, resulting in a total of 30k elements.

(a)

(b)

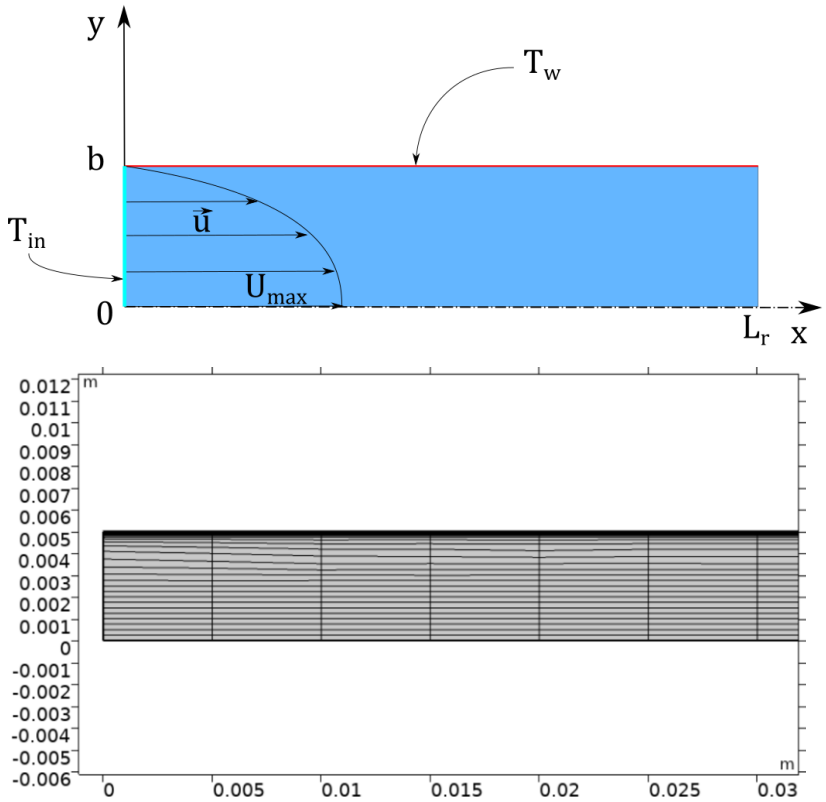

Figure 3 : Sketch of half of the channel showing the main boundary conditions (a) and mesh (b).

The Nusselt number values were evaluated at ten regularly spaced positions along the channel. The values start to decrease at the very beginning of the channel due to the thermal boundary layer and soon reach a constant value within the interval [7.45: 7.55]. This is very satisfactory considering that the reference value of 7.5 was obtained from Figure 2. Finally, the corresponding heat transfer coefficient was within the interval of 9.8 to 9.9 $W.m^{-2}.K^{-1}$. Consequently, the validation of the numerical model against the analytical value was deemed to be successful.

3. Design of the system

This section focuses on the design of the heat exchanger, which consists of the air channel, a concrete slab at the top, and PCM material at the bottom. The analysis is limited to heat transfer within the system and does not include heat transfer with the rooms located above and below. The objective of this study is to identify the key phenomena and the magnitude of heat transfer during the design stage. For this reason, a theoretical model of the material will be employed, and a simple energy balance will be considered.

3.1. Phase change modelling

Phase change modelling has been extensively studied in the scientific literature, with a variety of approaches having been proposed. A general approach was presented in (Voller and Prakash, 1987) and is often referred to as the enthalpy-porosity method. This process entails the calculation of the velocity field within the material through the resolution of the momentum balance and the consideration of natural convection. The introduction of a variable designated as porosity allows for the consideration of the change in viscosity that occurs concomitantly with phase change. (Lorente et al., 2014) provides an example of when natural convection can be the dominant mode for heat transfer. This may occur in the melted PCM if

the vertical dimension allows for it. In certain circumstances, however, conduction represents the primary mechanism for heat transfer, and the influence of natural convection can be deemed negligible. This phenomenon occurs when the PCM is micro-encapsulated, and in some configurations with macro-encapsulation, typically when the vertical dimension is small. In such cases, the heat transfer can be modelled by considering the energy balance exclusively, with the enthalpy h employed to incorporate the latent heat associated with phase change.

Assuming a constant density, the energy balance within the PCM can be written as follows (Tittelein et al., 2015) :

$$\rho \frac{\partial h}{\partial t} = -\boldsymbol{\nabla}(-\lambda \, \boldsymbol{\nabla} \mathrm{T}) \tag{5}$$

In the case of purely theoretical materials, phase change occurs at a specific temperature, which implies that the enthalpy is a non-linear function of the temperature. In contrast, for real materials, phase change occurs within a specific temperature range. In such a situation, the energy balance can be rewritten by introducing the apparent (or sometimes referred to as equivalent) heat capacity, denoted as $C_{p,PCM}(T)$, which includes the latent heat of fusion L_f:

$$\rho \, C_{p,PCM}(T) \, \frac{\partial T}{\partial t} = -\boldsymbol{\nabla}(-\lambda \, \boldsymbol{\nabla} \mathrm{T}) \tag{6}$$

As outlined by (Al-Saadi and Zhai, 2013), this approach has gained popularity due to its ability to address the temperature as the sole primary variable. A further advantage is that it can be readily incorporated into general programming software, such as COMSOL. Nevertheless, this approach is inadequate for capturing the hysteresis associated with phase change, which is a behaviour often observed with real PCM. It is recognised that the hysteretic behaviour has an impact on the kinetics of heat transfer in real applications, as discussed in (Barz and Sommer, 2018). In the latter study, a fine modelling of the hysteresis was introduced and shows a very

good agreement with experimental results obtained under different temperature cycles. However, the model uses some parameters that have to be fitted to experimental results, which means that the material has already been selected. For this reason, neglecting hysteresis at the early design stage of a heat exchanger seems a reasonable assumption.

In the present paper, the material is assumed to undergo a phase change within a specific temperature range, ΔT_{Melt}, centred around the average melting temperature, T_{Melt}, and hysteresis effects are neglected. The heat capacity increases to account for the latent heat of fusion that is spread throughout this range. Beyond this range, the specific heat capacity remains constant and is denoted as $C_{p,PCM,0}$.

$$C_{p,PCM}(T) = C_{p,PCM,0} + \frac{L_f}{\Delta T_{Melt}} SF(T) \tag{7}$$

Where $SF(T)$ is a step function that equals 1 when the temperature is within the melting range ΔT_{Melt} and 0 otherwise. Note that the edges of the step have been smoothed to avoid numerical issues at the beginning and end of the phase change. Other mathematical models have been used in the literature for similar purposes, such as a Weibull density function in (Barz and Sommer, 2018), a combination of polynomial functions in (Guermat et al., 2024) or of Gaussian functions (Alvarez-Rodriguez et al., 2024). In most cases, the coefficients of such functions have been identified from DSC measurements (Differential Scanning Calorimetry), but this implicitly means that the PCM material has already been selected.

The model proposed in this paper was employed for the purpose of making a comparison with the published results of (Guermat et al., 2024). In their study, the authors employed COMSOL to model a composite wall comprising 2 cm of PCM, subjected to the outdoor conditions of the Algerian city of Tamanrasset. The simulation was executed for a period exceeding 2000 hours, during which detailed temperature values were presented over a duration of 100 hours. This

period coincided with a period of elevated outdoor temperatures and significant solar loads, with peak values exceeding 1000 W.m^{-2}. The principal distinction between the model put forth by (Guermat et al., 2024) and the one employed in the present study is that the former solved the momentum equation for the PCM. The simulation results are compared in Figure 4.

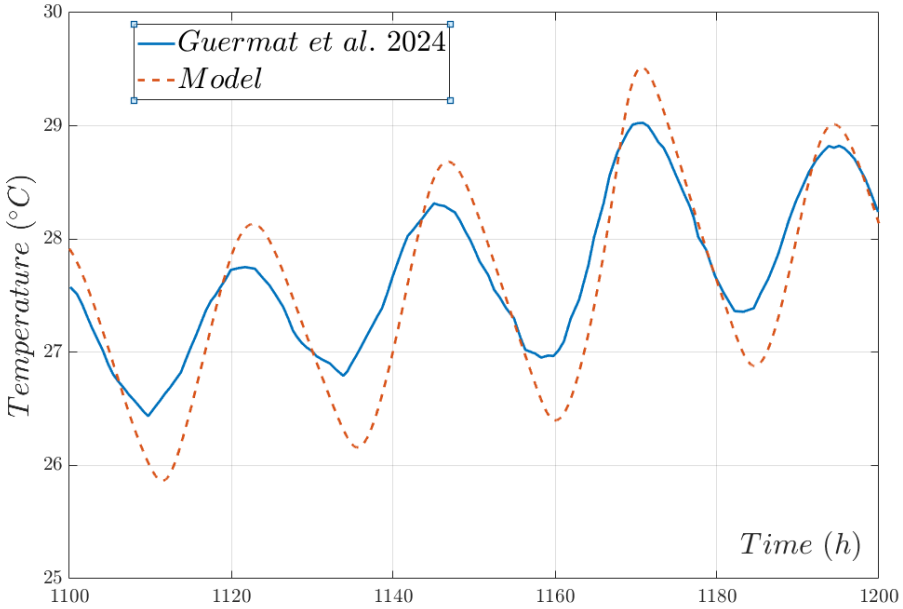

Figure 4. Comparison of the temperature of the indoor surface of a multilayer wall that includes a 2 cm thick layer of PCM.

The present model is capable of adequately reproducing the temperature variations obtained in the reference study. The Root Mean Squared Error (RMSE) for this simulation was approximately 0.4°C. In conclusion, the aforementioned comparison lends considerable support to the reliability of the proposed model in exploring the design of the system under consideration in the present paper.

The local melting fraction m_f is a measure of the liquid to solid quantities in the PCM. It can be calculated for each element using the following:

$$m_f = \frac{\int_{T_s}^{T} \left(C_{p,PCM}(T) - C_{p,PCM,0}\right) dT}{\int_{T_s}^{T_c} \left(C_{p,PCM}(T) - C_{p,PCM,0}\right) dT} \quad (8)$$

Where T is the temperature of each element, T_S is the temperature at which melting start and T_c is the temperature at which melting is completed.

Integration can be used to obtain the global melting fraction for a given surface (or volume in a 3D problem). For 2D problem this integral is as follows:

$$M_f = \frac{1}{L_{PCM}\, d_{PCM}} \iint m_f \; dx\, dy \tag{9}$$

Where d_{PCM} is the thickness of the PCM layer.

Therefore, the system aims to facilitate rapid changes in the global melting fraction M_f, which indicates effective exploitation of latent heat transfer. However, it is important to consider that sensible heat transfer also occurs. Thus, this aspect will also be covered within the discussion. It is proposed to rely on dimensionless temperature, θ, to depict progression towards thermal equilibrium, defined as:

$$\theta = \frac{T - T_{min}}{T_{max} - T_{min}} \tag{10}$$

3.2. System description and simulation considerations

The system is designed for refurbishment purposes. In office settings, it is typically installed beneath a 12 cm thick concrete slab ceiling, which serves as the upper part of the ventilation channel. Phase change materials (PCM) should be placed at the bottom of the channel, covering the same surface area as the ceiling. To account for real estate concerns, the PCM layer should be relatively thin. Macro-encapsulated solutions were considered as they offer an effective way to address density changes and the resulting risk for leaks.

Organic PCM with a wide range of heat transfer properties are now available on the market. Some of these materials are macro-encapsulated, as exemplified in Figure 5, using aluminium

containers and resulting in 1 cm thick panels. This choice is consistent with the findings of (Gallardo and Berardi, 2021). However, since this study focuses on the early design stage, it was decided not to focus on a specific product. Instead, average values inspired by two manufacturers ("PCM Products Ltd," n.d.; "Rubitherm," n.d.) were used. For the same reason, the material properties for concrete in the software's built-in library were used and are shown in Table 1.

Table 1. Material properties.

Properties	Concrete	PCM
ρ (kg.m^{-3})	2300	870
C_p (J.kg^{-1}.K^{-1})	880	1900
k (W.m^{-1}.K^{-1})	1.8	0.21
α (m^2.s^{-1})	8.9 10^{-7}	1.3 10^{-7}

When considering energy storage within the PCM and modelling it according to equation (7), the following values were used:

- The latent heat of fusion L_f was taken as 155 kJ.kg-1. According to (Mousavi et al., 2021), the value presented here is an intermediate value for organic PCM and is comparable to the performance of the PCM described in (Weinläder et al., 2014).
- The melting range ΔT_{Melt} was set to 2 K, although it is acknowledged that some organic materials may exhibit greater values.
- The specific heat capacity for the solid and fluid phases $C_{p,PCM,0}$ were considered identical and equal to 1900 J.kg^{-1}.K^{-1}.
- At this stage, the melting temperature has yet to be selected. For illustrative purposes, however, Figure 5 shows the modelled equivalent specific heat for a melting temperature of 17 °C.

To facilitate the analysis of heat transfer within the system, it was determined that maintaining consistent material properties throughout the study would be beneficial. Therefore, only the melting temperature was varied. Once the global design has been finalised, it is recommended that a parametric study be conducted with realistic material properties to refine the design and optimise its thermal performance.

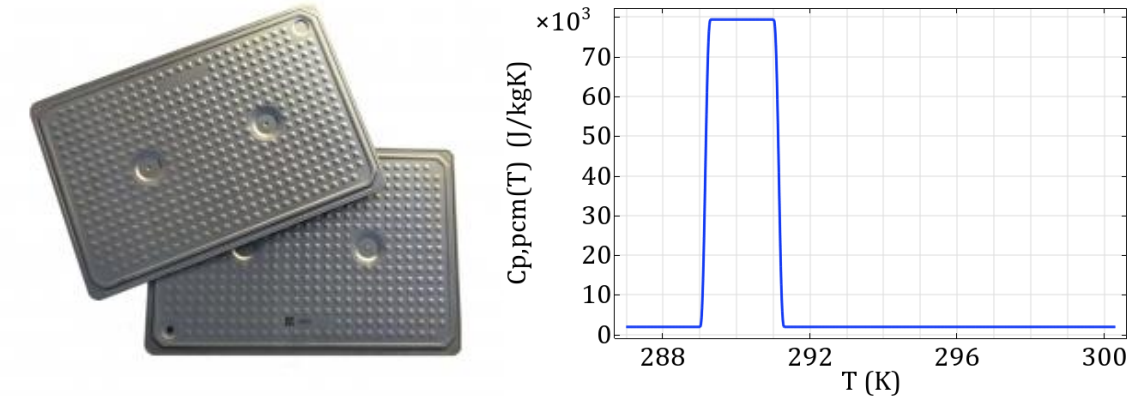

Figure 5. Example of macro-encapsulated PCM (left, ("Rubitherm," n.d.)) and modelled equivalent specific heat capacity for a melting temperature of 17°C (right).

Macro encapsulating material is generally of a very thin and highly thermally conductive nature. Additionally, the layer of PCM is 1 cm in thickness, which results in negligible convective heat transfer within the PCM. Consequently, this is consistent with the assumption previously made that natural convection can be disregarded.

The PCM layer was meshed in a similar manner to the air channel to ensure a precise estimation of the position of the melting front while larger elements were used for the concrete layer. The final mesh consists of 90k elements, with approximately one third allocated to each layer. In contrast to the study of the channel, this study considers a time-dependent approach. To investigate the kinetics of phase change within the system, a homogeneous initial temperature was set throughout the system at the lower threshold for phase change (*e.g.* 289.15 K in the case of Figure 5). Finally, a variable time step technique was selected. However, the time step had to be limited to a higher threshold of 3 minutes to ensure consistency.

3.3. Kinetic of phase change

A parametric study was carried out on the temperature at the channel inlet, T_{in}, by selecting values ranging from 3 to 11 K above T_{Melt}, and denoted $\Delta T_{C\text{-}M}$. The results were analysed from different perspectives: first, at a global scale to determine the time it takes to melt the entire PCM or a fraction of it, and then at a local scale to examine the dynamics more closely. In relation to this specific point, it is worth noting that (Tarzia, 2004) proposed an analytical solution for 1D heat transfer. Assuming that phase change occurs at a specific temperature rather than over a melting range and that the convective heat transfer coefficient is sufficiently high, the solid-liquid front *s(t)* would be a function of the square root of time, as follows:

$$s(t) \propto \sqrt{t} \tag{11}$$

The phase change kinetics were compared for all inlet temperature values. The results are presented in Figure 6, using dimensionless values such as the global melting fraction (M_f) on the *y-axis*. The abscissa represents dimensionless time, $\widetilde{t_M}$, defined as the ratio of time against the time for complete melting for each inlet temperature. This means that complete melting was achieved at different times, and therefore the denominator value changes according to T_{in}. Assuming 1D heat transfer, equation (11) can be normalised by the total thickness of the material and the time for complete melting, leading to a theoretical kinetic that also follows a square root function.

$$M_f(t) \propto \sqrt{\widetilde{t_M}} \tag{12}$$

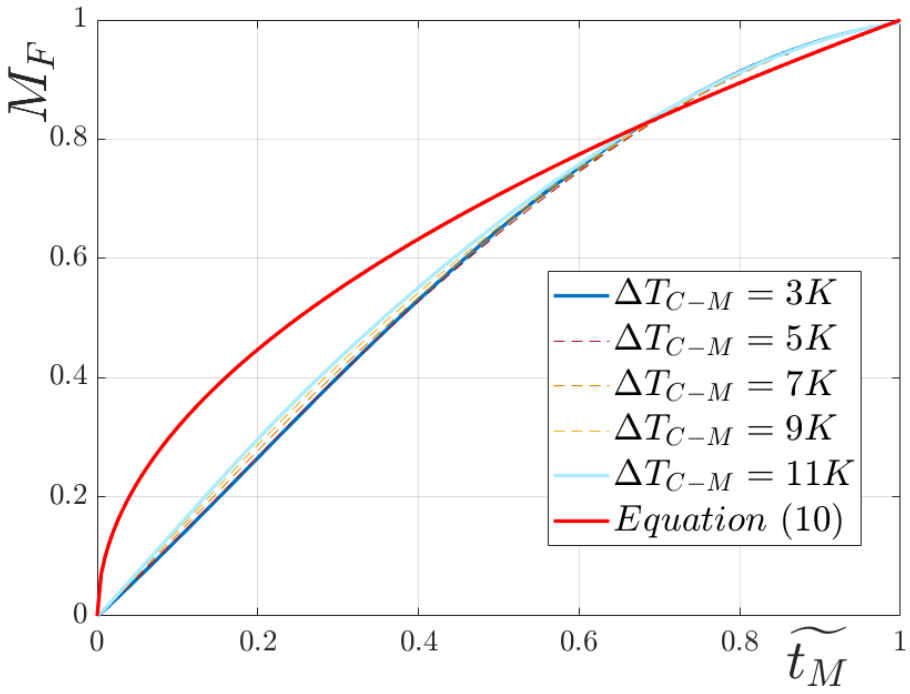

Figure 6. Global melting fraction M_f as a function of dimensionless time to complete melting for various inlet temperatures.

Figure 6 shows that the temperature at the inlet only slightly affects the kinetic for melting, despite the non-linearity introduced by phase change. For instance, at approximately $\widetilde{t_M}$ equals 0.5, two-thirds of the PCM are completely melted, while the remaining third takes longer to melt completely. However, the shape of the curve differs from the theoretical solution for 1D heat transfer. The discrepancy may be explained by the convective coefficient obtained with the channel, which is not as high as assumed in the theoretical development of (Tarzia, 2004). However, this also suggests that 2D heat transfer may be involved.

As the global kinetic is not significantly affected by the inlet temperature, heat transfer can be examined independently of it. It was chosen to present the results obtained when all the PCM was completely melted over 25% and 75% of the total length, designated L_{m25} and L_{m75} respectively, for $\Delta T_{C\text{-}M} = 7$ K. The local melted fraction is plotted on top of Figure 7, while the plots at the bottom represent the dimensionless temperature in the entire system. Note that

the plots are scaled differently on the vertical and horizontal axes to aid visualization and that the system is actually 5 m long and 0.14 m thin.

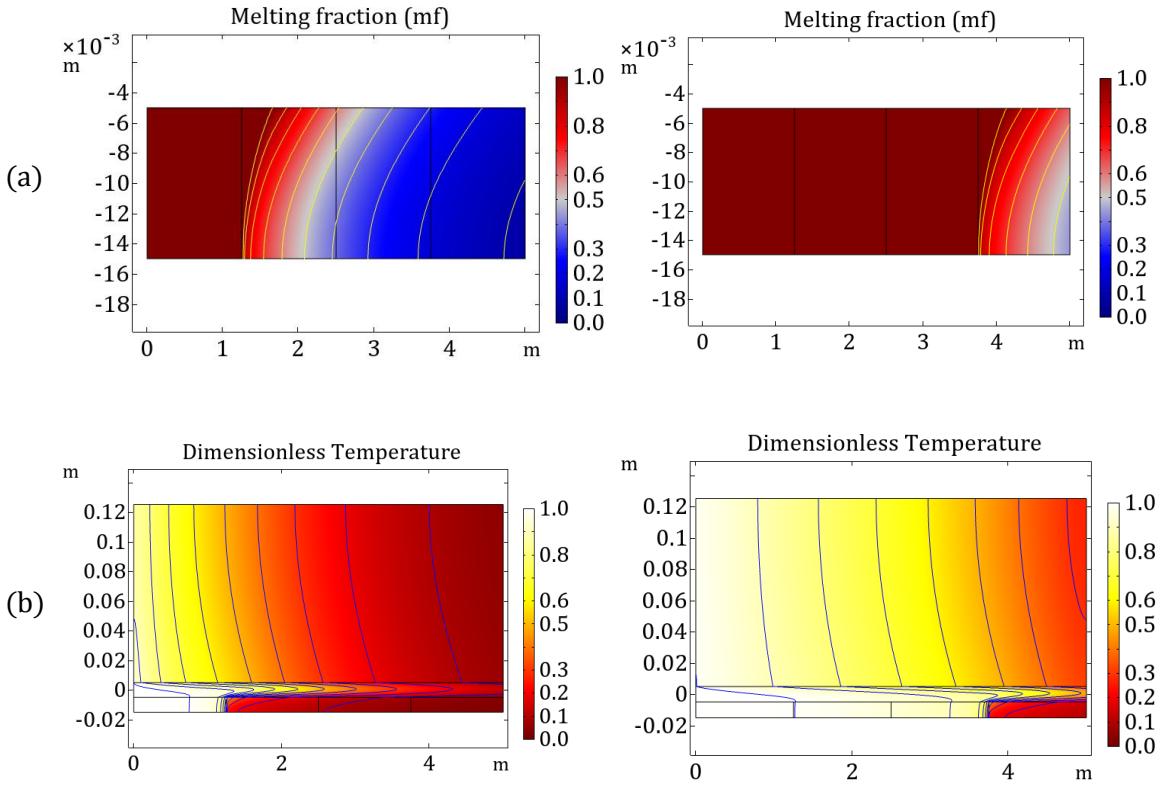

Figure 7. Local melting fraction m_f obtained in the PCM (a) and dimensionless temperature θ obtained over the entire system (b) for $\Delta T_{C\text{-}M} = 7$ K for L_{m25} and L_{m75}. The black lines represent isotherms.

Melting is observed across a large surface of the PCM, with melting fractions ranging from 0 to 1. However, the melting fraction varies significantly depending on the position, indicating an inhomogeneous ratio of fluid to liquid. When melting is almost complete at a given position, it is only half completed between 1 and 2 metres further in the channel. The constant melting fraction position, which follows an isotherm, is not vertical but tilted with a slope of approximately 1/100. This means that it is almost horizontal (Figure 7 is not to scale). However, this slight slope moves progressively from the inlet to the outlet of the channel. Therefore, the analytical solution proposed by (Tarzia, 2004) cannot be applied here.

Heat transfer is more intense near the liquid front, where the melting fraction is nearing unity. This is evident from the greater temperature variations observed at this location. As the melting front approaches the end of the channel, there is still a variation of the local melting fraction on the vertical axis, indicating slow heat diffusion in this direction due to the phase change and low thermal conductivity.

Considering the entire system, a distinct dynamic can be observed by examining the dimensionless temperature. The melted (liquid) portion of the PCM exhibits a uniform temperature, followed by a sudden temperature drop at the melting front compared to concrete, and that is the consequence of the phase change. However, a more regular temperature gradient can be observed in the concrete slab above, in the direction of the airflow. Although heat diffusion appears to be more progressive in concrete, the asymptotic value is reached at an abscissa that is smaller than that of the PCM, at a specific time. This indicates a slower kinetic for heat diffusion in the concrete slab.

The impact of the temperature difference between the air at the inlet and the melting temperature is then analysed. It is a trivial fact that a higher temperature difference results in faster melting, while the global (dimensionless) kinetic remains constant as depicted above. Figure 8 provides a better understanding of the melting process by showing the time required to achieve complete melting of a given fraction of the total length. Note that the illustrations provided in Figure 7 correspond to L_{m25} and L_{m75}.

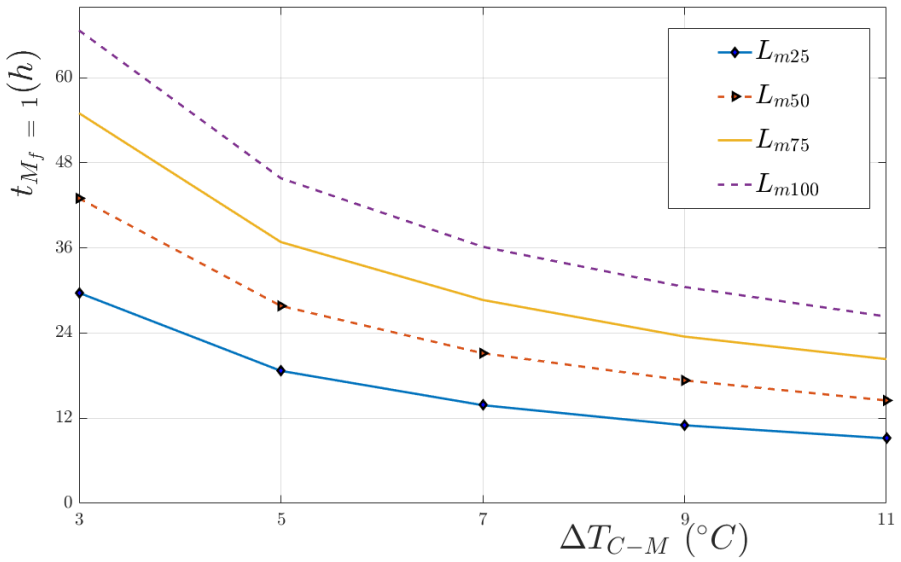

Figure 8. Time required to achieve complete melting over a fraction of the total length for given temperature differences between channel inlet and melting temperature.

It has been found that in all cases, it takes more than 24 hours to completely melt the PCM. This raises concerns about using such a system in an office environment. A cyclic pattern is foreseen where heat should be stored and released within 24 hours. Hence, it is clear that achieving complete melting and solidification cycles is not possible with this design, at least for the temperature being considered. It can be concluded that using PCM over the entire length would be economically inefficient due to its high cost compared to more conventional construction materials. (Royon et al., 2014) reached a similar conclusion for the particular geometry of a hollow concrete floor panel. It was found that for a given temperature cycle, the amount of PCM placed in the cores could be reduced by half to mobilise more of the phase change potential. (Weinläder et al., 2014) also examined PCM that covers about half of the ceiling surface. For the current study, it would be preferable to place PCM at the beginning of the duct and use another material downstream, such as gypsum board or a wood panel.

3.4. Behaviour of the system for cyclic temperature variation at the inlet

For the rest of this study, it was proposed to use phase change material (PCM) for only 50% of the length due to its ability to completely melt in less than 15 hours, as depicted in Figure 8. For the second half of the channel, PCM was replaced by a fictitious material that has exactly the same thermal properties except for the latent heat, the latter being set to zero, in order to facilitate the analysis of the results. For convenience, it will be referred to as 'plaster' even though the properties of real plasterboards may differ.

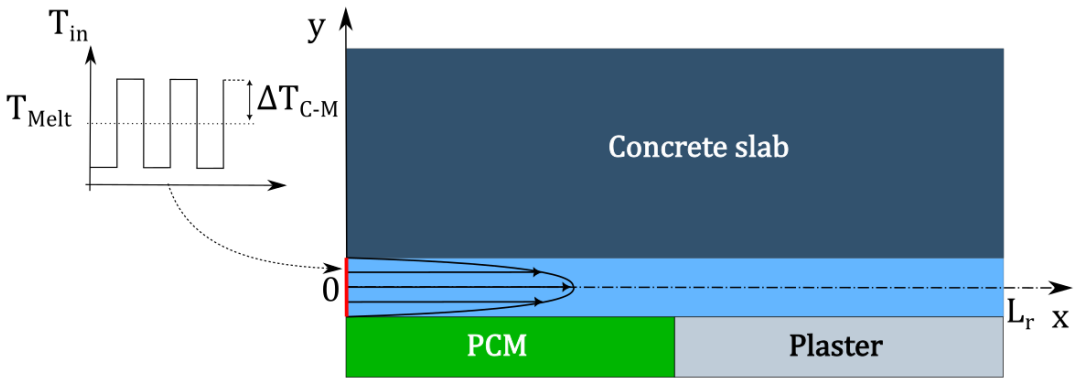

Figure 9. Sketch of the system containing PCM and plaster at the bottom of the air channel.

The thermal behaviour of the system was examined under periodic conditions defined over a 24-hour period, as illustrated in Figure 9. The temperature at the inlet of the channel underwent step changes every 12 hours. The average air temperature, T_{in}, corresponds to the melting temperature of the PCM, and a parametric study was carried out by changing the amplitude of the steps, denoted $\Delta T_{C\text{-}M}$, ranging from 3 to 11 K similar to the study in the previous section.

Nevertheless, a reduction in the quantity of PCM by half raises questions about the fundamental concept of the system. It can be observed that an increase in $\Delta T_{C\text{-}M}$ would have a significant impact on the potential for sensible energy storage within the system, while the potential for latent energy storage would remain the same. These considerations were used to

compute the values presented in Table 2, in which the total energy stored in an ideal cycle, E_{Tot}, is presented against the tested values of $\Delta T_{C\text{-}M}$. In this context, the term "ideal cycle" refers to a sufficiently long cycle that allows for the attainment of a steady state in heat transfer. The second column presents the ratios obtained by comparing the sensible energy stored within the concrete (E_{Con}) with the latent energy storage, E_{Lat}. The same calculation was repeated for the next two columns, utilising the total energy stored within the PCM (E_{PCM}), which encompasses sensible energy.

Table 2. Energy storage potential of the system for an ideal cycle, and comparison to the potential for latent energy storage.

$\Delta T_{C\text{-}M}$ K	E_{Tot} (MJ)	$\frac{E_{Con}}{E_{Lat}}$	$\frac{E_{PCM}}{E_{Lat}}$	$\frac{E_{Tot}}{E_{Lat}}$
3	2.18	2.16	1.07	3.23
5	3.19	3.60	1.12	4.72
7	4.98	5.04	1.17	6.21
9	6.02	6.48	1.22	7.70
11	7.06	7.92	1.27	9.19

It seems that the concrete slab has a considerable potential for heat storage, due to its substantial thickness and high thermal mass in comparison to the PCM. The potential for sensible energy storage is significantly greater than that of PCM, even for low values of $\Delta T_{C\text{-}M}$, with the capacity exceeding that of the PCM by a factor of more than two for a temperature change of only 3K. Additionally, the potential for sensible heat storage increases linearly with $\Delta T_{C\text{-}M}$, which contrasts with the case of latent energy in the context described above. These elementary considerations demonstrate that, although PCM remains a viable option in the context of refurbishment, it should be noted that the proposed solution may also rely on the slab's capacity for heat storage, analogous to ventilated slabs.

Next, the computational work is carried out over several 24-hours cycles, and only the results of the final cycle are analysed to ensure independence from the initial conditions. The global melting fraction is presented in Figure 10 and numerical values are detailed in Table 3.

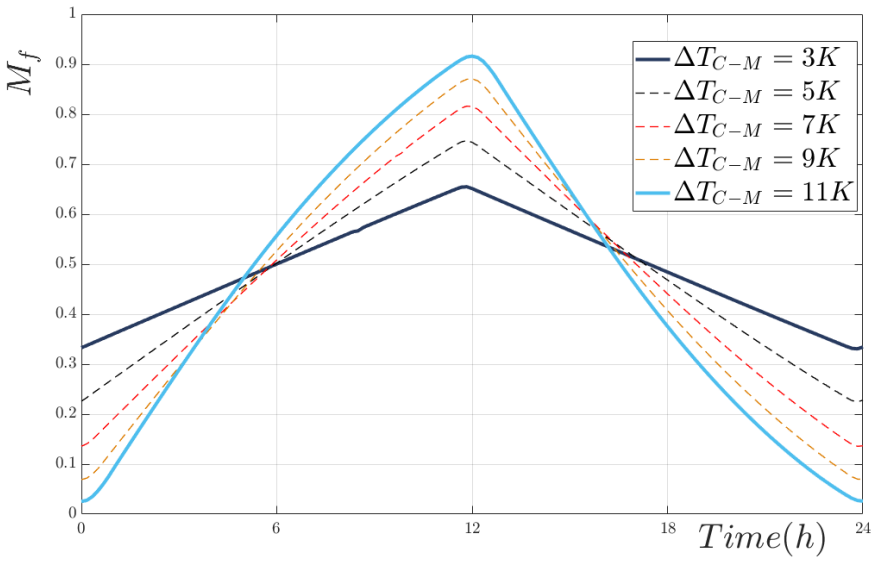

Figure 10. Global melting fraction obtained for cyclic boundary conditions at the inlet of the channel and different temperature amplitudes. PCM was employed over 50% of the system length.

Table 3. Global melting fraction, average dimensionless temperature in concrete and fraction of total to latent energy stored in the system for a 24-hour cycle.

ΔT_{C-M}	M_f			$\bar{\theta}$	$\frac{E_{Tot}}{E_{Latent}}$
(K)	Max	Min	Δ	Δ	
3	65.5 %	33.1 %	32.4 %	16.7 %	2.14
5	74.7 %	22.5 %	52.2 %	17.0 %	2.23
7	81.6 %	13.6 %	68.1 %	17.6 %	2.40
9	87.1 %	6.9 %	80.1 %	18.3 %	2.62
11	91.6 %	2.6 %	89.0 %	18.9 %	2.88

The global melting fraction exhibits high variations when the magnitude of the temperature at the inlet of the channel exceeds 7 K where it reaches 68% and is nearing 90% at 11 K. It shows that the design of the modified system is effective at using the latent heat potential of PCM, for 24-hour cycles at least. Secondly, the amplitude of the temperature steps has a noticeable

impact on the activation of latent heat storage, but it has a negligible effect on the dynamics of sensible heat storage within the concrete slab. This is illustrated in Table 3, where the amplitude of the dimensionless temperature of the concrete remains between 16 and 19%, indicating that sensible heat storage is not yet at its maximum. This can be explained by the fact that latent heat transfer is triggered at a fixed temperature, which introduces non-linearities in heat transfer within the PCM. However, the phenomenon remains linear within the concrete slab and is slightly affected by the temperature of the materials located at the bottom of the channel due to the airflow. Consequently, the sensible heat storage during a cycle is considerably less pronounced than the values presented in Table 2. Nevertheless, it remains a notable phenomenon. It is greater than latent heat storage, regardless of the temperature amplitude employed at the inlet of the channel.

It can be concluded that an acceptable design is obtained when an idealized PCM material was employed over half the length of the channel since it maximises phase change when exposed to temperature steps at the inlet. Conversely, the sensible energy storage potential in concrete was found to be high but inefficiently utilised, irrespective of the amplitude of the temperature steps used for 24-hour cycles.

4. System exposed to the room temperature at its bottom surface

Previously, the system was viewed independently from the office it was installed in. The main purpose of using PCM is to store and release energy, but the objective of the system is broader. It is installed below the ceiling to facilitate heat transfer with the room and to contribute to more comfortable indoor conditions, similar to radiant panels or ventilated slabs. Therefore, the room temperature affects the heat balance of the system, and its design must be adjusted accordingly. This section considers a constant room temperature for simplification, while the

system is exposed to cyclic step temperature variation at its inlet. The analysis will separate the melting and solidification phases. Finally, the cooling power provided to the room and the potential for phase change will be discussed.

4.1. Theoretical considerations

As previously stated, the designed system shares similarities with radiant panels as a large chilled surface is exposed to the indoor environment. However, it is important to note that the dewpoint temperature of indoor air poses a significant limitation for the use of radiant cooling panels. This is due to the fact that cooling occurs through the exposure of a chilled surface to the indoor environment, where condensation may occur and cause water to drop on users, which is unacceptable. Consequently, the cooling power is restricted by indoor conditions (Rhee et al., 2017). The same phenomenon applies to the lower surface of the system. For this study, indoor conditions of 25°C and 50% relative humidity were considered, resulting in an indoor dew point temperature slightly lower than 14°C. To reduce the risk of condensation, we follow the recommendation of (Feustel and Stetiu, 1995) and add a safety margin of 2 K, resulting in a minimum surface temperature of 16°C.

To prevent low temperatures on the surface that comes into contact with indoor air, an additional layer can be added below the PCM. This layer provides extra thermal resistance, referred to as R_{Ins}, but also offers the possibility of improving acoustic absorption. Poor acoustic quality is commonly experienced with radiant ceilings, as mentioned in (Karmann et al., 2018). Macro-encapsulation is achieved using a metallic material, which is often not effective at absorbing acoustic waves. Adding insulating material at the bottom of the system may provide benefits because of its porous nature. However, this paper will focus solely on heat transfer and will not discuss the exact nature of the material or its impact on acoustics.

To model this additional layer, a pure thermal resistance was considered, and the heat transfer coefficient at the bottom of the system, h^*, was defined as follows:

$$h^* = \frac{1}{\frac{1}{h_T} + R_{ins}} \tag{13}$$

The total heat transfer coefficient introduced in this equation, h_T, combines convective and radiative heat transfer. The value of the latter has been fixed at 11 $W.m^{-2}.K^{-1}$ to comply with the REHVA standard, which is an intermediate value in the figures reviewed in (Shinoda et al., 2019).

Considering heat transfer with the room is not limited to the condensation risk, it also implies that the dynamic of heat transfer within the system is modified, especially for the PCM as it is the most exposed element. In the context of cooling, solidification of the PCM is especially influenced because the heat flux coming from the room will slow or even inhibit phase change. Therefore, a parametric study was made in order to highlight the influence of the added thermal resistance. Results are presented in Figure 11 for steady state, which stands as a limit situation, and for several temperature difference between the room and the air at the inlet of the channel $\Delta T_{R\text{-}C}$.

(a)

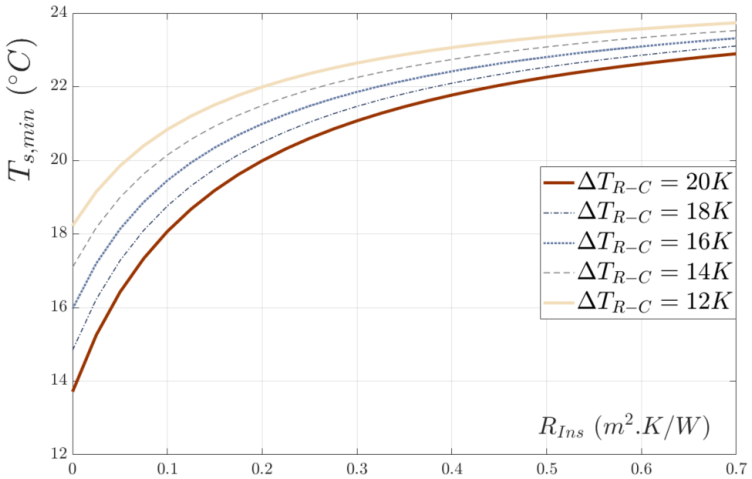

(b)

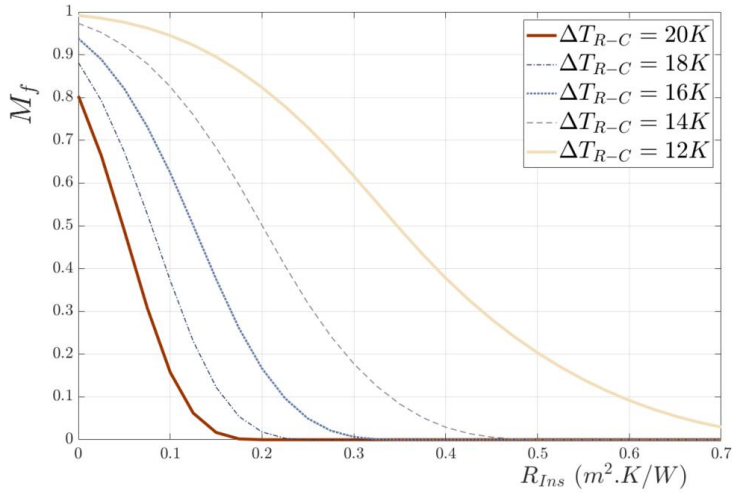

Figure 11. Minimal ceiling temperature (a) and global melting fraction (b) obtained at steady state for a given additional thermal resistance and inlet channel temperature.

In most cases, the risk of condensation can be easily eliminated by adding a thin thermal resistive layer. For example, a resistance of 0.05 $m^2.K.W^{-1}$ would be required in the worst case, and this can be achieved with only 2 mm of mineral wool. From a practical standpoint, it can be observed that the PCM would be situated on a frame, thereby introducing a thermal resistance, regardless of the nature of the frame and the boundaries. Therefore, it is safe to conclude that the risk of condensation can be easily handled for this system.

Secondly, it is important to note that heat transfer with the room significantly affects the global melting fraction. When no thermal resistance is present, the PCM remains mostly melted at all temperature differences considered here, which is undesirable. A first solution would be to provide a colder air to the channel to force solidification. However, it is anticipated that this solution is undesirable for two reasons Firstly, it is important to note that solidifying the PCM is a necessary step, but it should not be the primary objective. The main objective is to maintain the room temperature within a comfortable range. To be more general, the system should be designed to release energy as much as possible during solidification, but this should be achieved with a minimal influence on the room temperature. This is because solidification is scheduled when there is no occupancy, meaning that the cooling demand for the room is low or

even null. Nevertheless, as heat transfer occurs through the PCM, the cooler the supplied air temperature, the greater the cooling power provided directly to the room. Consequently, providing a colder air would increase the mismatch between the energy production and its usage. A second reason that makes this solution undesirable, yet to a lesser extent, is that generating a very cold air also results in dry air blown into the room. Given the air change rate and typical moisture sources in offices, it is anticipated that the resulting indoor relative humidity will be within an acceptable range. However, it is possible that discomfort may be experienced locally due to the dry air.

Instead, it is worth considering a resistive thermal layer, which does not have these drawbacks. However, a minimum temperature difference of 16K seems preferable because the thermal resistance required to maintain solidification increases rapidly. In practice, achieving the required thickness of the resistive layer might be quite easy, but a high thermal resistance also isolates the system from the room, which is a primary goal. Finally, it is important to note that Figure 11 provides only a minimal value for the thermal resistance, as it was obtained for steady state conditions. As an initial estimate, the resistance that permits achieving less than 2% of liquid fraction is retained as a reference value, which can be increased and utilised for subsequent time-dependent studies.

To summarise the results obtained previously, the final system should include:

- A 1 cm thick air channel to combine a fair convective heat transfer coefficient with a large exchange surface.
- A 1 cm thick layer of PCM, spread over half of the length of the ceiling (2.5 m here) to maximise surface exposure to the indoors and minimise the quantity of PCM installed.
- A channel inlet to melting temperature difference $\Delta T_{C\text{-}M}$ greater than 7K to maximize the use of latent heat potential during 24-hour cycles.

- A channel inlet to room temperature difference ΔT_{R-C} twice as high as ΔT_{C-M} is foreseen to facilitate melting and solidification. However, a high threshold of 20K is proposed to avoid promoting temperatures that would lead to discomfort and condensation issues due to excessively low temperatures.
- A minimal thermal resistance, $R_{ins,min}$, which definition relies on ΔT_{R-C} and that allows for reaching 98% of solidification at steady state. It is anticipated that higher resistances will be necessary to achieve efficient phase change under cyclic conditions.

Table 4 presents the definition of three cases that differ slightly based on the aforementioned considerations. It should be noted that, from a practical standpoint, the minimal thermal resistance could be achieved by a 5 cm thick layer of plaster or a 1 cm thick layer of lightweight wood panel.

Table 4. Parameters retained for the 3 cases.

Case	ΔT_{R-C} K	$R_{Ins,min}$ $m^2.K.W^{-1}$	T_{melt} °C	ΔT_{C-M} K
1	20	0.15	15	10
2	18	0.20	16	9
3	16	0.275	17	8

To analyse the behaviour of the system exposed to room temperature, we propose distinguishing between the periods of solidification or melting. First, we consider solidification and apply a heat balance to the air channel, which leads to:

$$\dot{m}\, C_{p,a}\, T_{in} + \phi_{Con} + \phi_{PCM} = \dot{m}\, C_{p,a}\, T_b \qquad (14)$$

Where T_b is the temperature of the air at the outlet of the channel and blown into the room, ϕ_{Con} is the heat flux released from the concrete slab and transferred to the air channel and ϕ_{PCM} the heat flux transferred from the PCM. The heat flux transferred with the plaster is

included in the latter for the sake of simplification of the equations. It is important to note that concrete can only exchange heat with the air channel, meaning ϕ_{Con} is, in absolute value, the variation of sensible energy contained with concrete, denoted ϕ_R^{Con}. On the other hand, PCM exchanges heat with the air channel and another heat flux is also transmitted to the room (ϕ_t). Applying a heat balance to the PCM yields:

$$-\phi_{PCM} + \phi_t = \phi_R^{PCM} \tag{15}$$

Where ϕ_R^{PCM} is the variation of heat within the PCM. The equation (14) and (15) can be combined to determine the heat flux released within the entire system, ϕ_R.

$$\begin{gathered} \dot{m}\, C_{p,a}\, (T_{in} - T_b) = \phi_R - \phi_t \\ \phi_R = \phi_R^{Con} + \phi_R^{PCM} \end{gathered} \tag{16}$$

Then, insert the flux leaving the room due to the airflow rate at temperature T_r, so that the equation becomes:

$$\begin{gathered} \phi_{in} = \dot{m}\, C_{p,a}\, (T_{in} - T_r) \\ \phi_b = \dot{m}\, C_{p,a}\, (T_b - T_r) \\ \phi_R - \phi_t + \phi_b = \phi_{in} \end{gathered} \tag{17}$$

The main elements are depicted in Figure 12. All terms in equation (17) are negative during solidification, except ϕ_t which represents the heat flux absorbed by the PCM. Considering its reciprocal value, $\phi_t{}'$, which represents the heat flux leaving the room, and normalising (17) by ϕ_{in}, there are three terms that add up to unity. These terms represent the proportion of the cooling power provided to the room that is transferred to the system (equivalent to the heat flux that is released), transmitted by conduction through the ceiling, or blown directly into the room.

$$\frac{\phi_R}{\phi_{in}} + \frac{\phi_t{}'}{\phi_{in}} + \frac{\phi_b}{\phi_{in}} = 1 \qquad (18)$$

Some of the heat fluxes are already calculated within the model (ϕ_t, ϕ_R) or directly estimated using their definition (ϕ_{in}). The only exception is the heat flux blown into the room, ϕ_b, which is estimated as follows:

$$\phi_b = \int_{-b}^{b} \rho_a \, C_{p,a} \, W_c \, u(y) \, (T(L,y) - T_r) \, dy \qquad (19)$$

Due to the dynamic nature of heat transfer in the system, the ratios presented in equation (18) vary during solidification. To simplify the analysis, they were averaged over the duration when the temperature at the inlet of the channel was low, which is half a period (12 hours). This is exemplified below for the fraction of heat flow rate that is blown into the room, F_b.

$$F_b = \frac{2}{\mathrm{T}} \int_0^{\mathrm{T}/2} \frac{\phi_b}{\phi_{in}} \, dt \qquad (20)$$

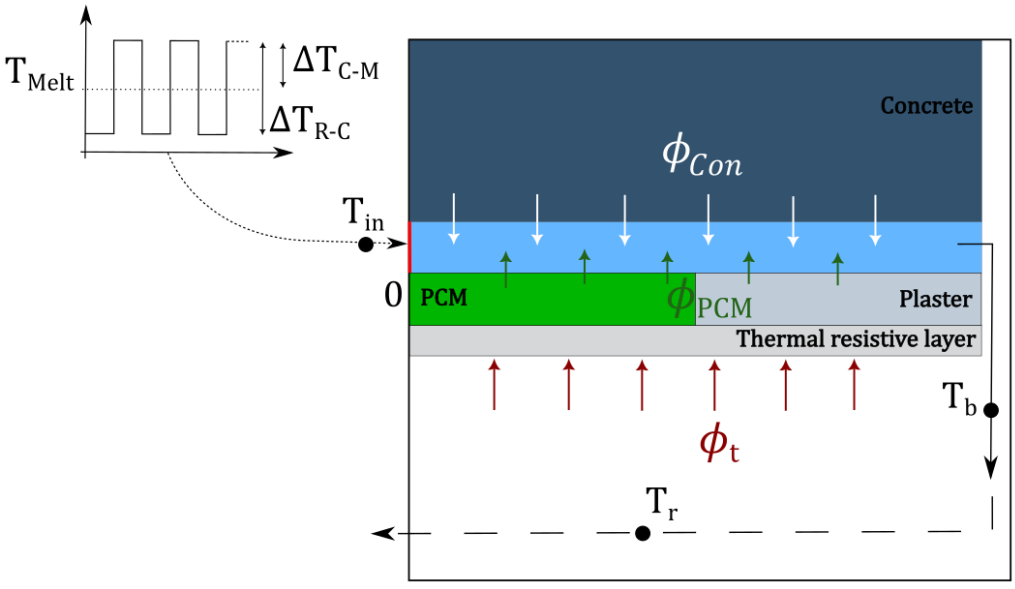

Figure 12. Sketch of the final system with identification of the heat fluxes.

The system's primary objective during melting is to cool the room, which is maintained at 25°C for simplification purposes. As the inlet temperature of the channel is the same as the room temperature, the heat balance of the system during melting yields:

$$\phi_R + \phi_t{}' + \phi_b = 0 \tag{21}$$

The mean value and standard deviation of the cooling power were analysed over a period of 12 hours. The cooling power is the sum of the heat flux blown into the room, ϕ_b, and exchanged with the bottom surface of the system,$\phi_t{}'$. The total amount of energy absorbed by the system, denoted as E_{tot}, was obtained by integrating the cooling power.

4.2. Results analysis

The simulations were repeated for the three cases presented in Table 4, and a parametric study was conducted by increasing the minimum value of the thermal resistance, $R_{ins,min}$, by a factor ranging from two to four. It should be noted that, from a practical standpoint, the maximal thermal resistance could be achieved by a 5 cm thick layer of polystyrene. Table 5 shows the results obtained when periodic state was reached. This implies that the simulations were conducted over multiple cycles and that the results were presented for the final cycles, during which no significant difference was observed between consecutive cycles. Note that the average cooling power during melting is provided along with its standard deviation.

Table 5. Results obtained for the system tested under various parameter configurations and exposed to room ambiance and 24-hour cycles.

Case	R_{ins}	Solidification			Melting		ΔM_f
		F_b	F_t'	F_R	P (kW)	E_{tot} (kWh)	
1	$R_{Ins,min}$	30%	33%	37%	-0.39±0.12	-4.54	0.28
	2 $R_{Ins,min}$	35%	24%	41%	-0.43±0.12	-5.04	0.45
	3 $R_{Ins,min}$	38%	19%	43%	-0.46±0.11	-5.32	0.56
	4 $R_{Ins,min}$	40%	16%	44%	-0.47±0.10	-5.49	0.63
2	$R_{Ins,min}$	32%	29%	39%	-0.37±0.11	-4.28	0.33
	2 $R_{Ins,min}$	37%	21%	43%	-0.41±0.10	-4.73	0.50
	3 $R_{Ins,min}$	39%	16%	45%	-0.43±0.09	-4.96	0.59
	4 $R_{Ins,min}$	41%	13%	46%	-0.44±0.08	-5.08	0.64
3	$R_{Ins,min}$	34%	25%	41%	-0.34±0.10	-4.02	0.38
	2 $R_{Ins,min}$	39%	16%	45%	-0.38±0.08	-4.39	0.54
	3 $R_{Ins,min}$	41%	12%	46%	-0.39±0.06	-4.54	0.61
	4 $R_{Ins,min}$	43%	10%	47%	-0.40±0.05	-4.62	0.65

During solidification, the aim is to maximise the fraction of heat released by the system, F_R, defined as in equation (16). In all tested configurations, this fraction ranges from 37% to 47%, indicating that most of the cooling power supplied to the system is transferred to the room either through the ceiling or because the air exits the channel at a low temperature. This ratio is in line with the results of (Weinläder et al., 2014), where it was found that about one third of the cooling power was supplied to the room through the airflow under similar operating conditions. The three fractions are fairly balanced when the minimum thermal resistance is employed. Increasing the thermal resistance reduces the fraction of heat flux transmitted to the room, which is the intended effect. However, this also results in more cooling power being provided to the room through the air channel outlet, whereas the energy released by the system only increases slightly. This trend is consistent across all three cases, although the fraction of released power is slightly greater for lower temperature differences and melting temperatures (case 3). In addition, further calculations were made by increasing the airflow rate, yet these are not presented in the manuscript. It quickly became apparent that switching

to turbulent flow within the same system was not a viable solution, as the fraction of heat blown into the space, F_b, increased at the expense of a decrease in the other two fractions.

During melting, it was found that the average cooling power is modest, ranging from 340 to 470 W and exceeding 500 W at the beginning of this phase. This leads to an average power density magnitude of approximately 30 $W.m^{-2}$. Such a value is consistent with the highest values experimentally obtained by (Gallardo and Berardi, 2022) for a suspended ceiling that includes PCM and a hydronic system, and with the ones of (Weinläder et al., 2014) for a similar system applied to a room that is twice larger. However, it is clear that such a limited cooling power may not be sufficient to meet the cooling demand of a real office. Therefore, the designed system should be considered as a means to alleviate the cooling demand for other energy systems used in the same room. The stored energy is not insignificant though, ranging from 4 to 4.5 kWh, which is comparable to the findings of (Labat et al., 2014) where both the total mass of PCM and total energy were halved, and to the ones of (Weinläder et al., 2014) where they were approximately doubled. The present study also shows that increasing the thermal resistance $R_{Ins,min}$ results in a higher cooling power and greater stored energy (up to +20%) under the tested conditions. Furthermore, it results in a decrease in standard deviation of the average power throughout the entire period, resulting in a steadier cooling power.

Finally, Table 5's last column indicates whether the tested configuration benefits from phase change. It is important to note that the three cases were designed to result in 98% phase change at steady state. However, the observed results show that less than 40% of the PCM undergoes solid-to-liquid changes during 24-hour cycles when considering the minimum thermal resistance. Most of the material remains under-utilised, which is unsatisfactory. However, the fraction of phase change material (PCM) involved in the phase change process

increases rapidly when the thermal resistance is doubled or even tripled, and it exceeds 50% in all three cases.

4.3. Discussion

To summarize, the results suggest that a higher thermal resistance at the bottom of the system is beneficial for exploiting the properties of the PCM. However, the system was also designed to favour radiant heat transfer between the ceiling and the occupants in order to provide comfortable indoor conditions. This is inconsistent with a high thermal resistance, which aims to separate the thermal behaviour of the heat exchanger from the room. As a result, the thermal resistance can be regarded as a degree of freedom that should be used to orient the design of the system towards two possible options:

1. The system is to be used to store as much energy as possible, *e.g.* for peak shaving or demand control purposes. In this scenario, a high level of thermal insulation should be retained.
2. The aim of the system is to improve indoor conditions in the context of refurbishment, i.e. a cool and homogeneous temperature is desired for the ceiling. To achieve this, a lower thermal resistance is more suitable, and the amount of PCM installed can be reduced.

Depending on the selected option, a more refined design could be achieved. Excluding the parameters studied in the present paper, four prospects have been identified. Firstly, this study has so far used theoretical material properties, which was justified by the need for quick calculations in the early design phase. However, more reliable results would be obtained if real material properties were used. Note that this should be supported by more detailed modelling of heat transfer during phase change. Secondly, it was observed that more than 30% of the

cooling power provided during melting is not transferred to the solid elements and exits the channel (see Table 5). To improve this, it is suggested to add fins into the channel to increase convective heat transfer, as exemplified in (Labat et al., 2014). Next, including the room heat balance would be beneficial as it would provide more details on the system's contribution to the cooling demand. Below is a simple room balance provided for exemplification, similar to the proposal in (Labat and Hazyuk, 2023) in the context of ventilated slabs:

$$KV_r\rho_a C_{p,a}\frac{\partial T_r}{\partial t} = \phi_t + \phi_b + U_w A_w(T_{ext} - T_r) + \dot{Q}_L \quad (22)$$

Where V_r is the room volume, U_w is the thermal transmittance of the envelope and A_w its surface, $\dot{Q}_L$ represents the thermal loads of the building and K accounts for the heat accumulation in furniture and partition walls and can be estimated as proposed in (Johra and Heiselberg, 2017). This approach is simple, as it neglects the thermal inertia of the envelope. Furthermore, it is also likely that the objective of maximising the use of phase change may conflict with the need to maintain the room temperature, T_r, within a desired range. However, it shows that moving to the scale of the room introduces numerous new elements. The latter are specific to each case and, for this reason, should not be considered during the early stages of design as in the present paper.

Finally, the nature of the signal at the channel inlet was fixed but not discussed. It is very likely that a square signal is not optimal and could be modified to better utilize phase change while maintaining simultaneously comfortable indoor conditions. Early tests have shown that the behaviour of the whole system is complex and that a trial and error approach is insufficient to identify a time series for the temperature at the inlet of the channel that is adequate. This incites to rely on more advanced control techniques instead, such as a rule based logic as exemplified in (Mousavi et al., 2024). However, designing and implementing a control logic

often require a large amount of simulation, leading to consequent computational cost that could be even prohibitive for the present problem. This scientific concern can be solved by using simplified models, as exemplified in (Labat et al., 2021). However, most techniques are only suitable for linear problems. The use of phase change material introduces non-linearity, which makes it difficult to build lighter models yet not impossible as exemplified by (Lu et al., 2020; Mousavi et al., 2023). Consequently, the construction of a lighter model of the system represents a promising prospect for its development.

5. Conclusions

This paper presents a methodology for designing a simple heat exchanger to be placed beneath a concrete slab during the refurbishment of a small office. The main objective is to improve heat transfer between the existing concrete slab and a Phase Change Material (PCM). This will be achieved by placing the material below the slab, separated by a thin rectangular channel that spans the entire ceiling surface. Fundamental theoretical considerations suggest that a thin and wide channel is optimal for enhancing heat transfer between the fluid and the two materials. Additionally, idealized yet common material properties are considered and it was shown that placing the PCM over half the length of the channel achieves a trade-off between exploiting phase change at its highest potential and addressing economic concerns. It was demonstrated that the melting temperature should be between 15 to 17°C for effective cooling. The kinetics of heat transfer were also examined when the system was exposed to a room maintained at a constant temperature. A simple 24-hour temperature cycle at the channel inlet highlighted the need for an additional thermal resistance between the PCM and the room. It has been discovered that resistance plays a crucial role in the thermal behaviour of the entire system and can promote energy storage when it reaches a certain level. Conversely, lower

resistances should be chosen if a radiative heat flux through the ceiling is desired. Further research is required to develop a design that is suitable for a specific case. This should include the use of real material properties instead of idealised ones and the modelling of the heat balance of the room. Additionally, a control technique that maximises the use of latent energy while maintaining the indoor temperature within a desired range must be defined.

6. References

Al-Saadi, S.N., Zhai, Z. (John), 2013. Modeling phase change materials embedded in building enclosure: A review. Renew. Sustain. Energy Rev. 21, 659–673. https://doi.org/10.1016/j.rser.2013.01.024

Alvarez-Rodriguez, M., Alonso-Martinez, M., Suarez-Ramon, I., José García-Nieto, P., 2024. Numerical model for determining the effective heat capacity of macroencapsulated PCM for building applications. Appl. Therm. Eng. 242, 122478. https://doi.org/10.1016/j.applthermaleng.2024.122478

Barz, T., Sommer, A., 2018. Modeling hysteresis in the phase transition of industrial-grade solid/liquid PCM for thermal energy storages. Int. J. Heat Mass Transf. 127, 701–713. https://doi.org/10.1016/j.ijheatmasstransfer.2018.08.032

Bianco, N., Fragnito, A., Iasiello, M., Mauro, G.M., Mongibello, L., 2022. Multi-objective optimization of a phase change material-based shell-and-tube heat exchanger for cold thermal energy storage: experiments and numerical modeling. Appl. Therm. Eng. 215, 119047. https://doi.org/10.1016/j.applthermaleng.2022.119047

Ciancio, V., Salata, F., Falasca, S., Curci, G., Golasi, I., De Wilde, P., 2020. Energy demands of buildings in the framework of climate change: An investigation across Europe. Sustain. Cities Soc. 60, 102213. https://doi.org/10.1016/j.scs.2020.102213

Corgnati, S.P., Kindinis, A., 2007. Thermal mass activation by hollow core slab coupled with night ventilation to reduce summer cooling loads. Build. Environ. 42, 3285–3297. https://doi.org/10.1016/j.buildenv.2006.08.018

Dallaire, J., Adeel Hassan, H.M., Bjernemose, J.H., Rudolph Hansen, M.P., Lund, I., Veje, C.T., 2022. Performance analysis of a dual-stack Air-PCM heat exchanger with novel air flow configuration for cooling applications in buildings. Build. Environ. 223, 109450. https://doi.org/10.1016/j.buildenv.2022.109450

Di Perna, C., Stazi, F., Casalena, A.U., D'Orazio, M., 2011. Influence of the internal inertia of the building envelope on summertime comfort in buildings with high internal heat loads. Energy Build. 43, 200–206. https://doi.org/10.1016/j.enbuild.2010.09.007

Dolado, P., Lazaro, A., Marin, J.M., Zalba, B., 2011. Characterization of melting and solidification in a real-scale PCM–air heat exchanger: Experimental results and empirical model. Renew. Energy 36, 2906–2917. https://doi.org/10.1016/j.renene.2011.04.008

Elnagar, E., Gendebien, S., Georges, E., Berardi, U., Doutreloup, S., Lemort, V., 2023. Framework to assess climate change impact on heating and cooling energy demands in building stock: A case study of Belgium in 2050 and 2100. Energy Build. 298, 113547. https://doi.org/10.1016/j.enbuild.2023.113547

Feustel, H.E., Stetiu, C., 1995. Hydronic radiant cooling—preliminary assessment. Energy Build. 22, 193–205.

Gallardo, A., Berardi, U., 2022. Experimental evaluation of the cooling performance of radiant ceiling panels with thermal energy storage. Energy Build. 262, 112021. https://doi.org/10.1016/j.enbuild.2022.112021

Gallardo, A., Berardi, U., 2021. Design and control of radiant ceiling panels incorporating phase change materials for cooling applications. Appl. Energy 304, 117736. https://doi.org/10.1016/j.apenergy.2021.117736

Guermat, Z., Kabar, Y., Kuznik, F., Boukelia, T.E., 2024. Numerical investigation of the integration of new bio-based PCM in building envelopes during the summer in Algerian cities. J. Energy Storage 79, 110111. https://doi.org/10.1016/j.est.2023.110111

Johra, H., Heiselberg, P., 2017. Influence of internal thermal mass on the indoor thermal dynamics and integration of phase change materials in furniture for building energy storage: A review. Renew. Sustain. Energy Rev. 69, 19–32. https://doi.org/10.1016/j.rser.2016.11.145

Karmann, C., Bauman, F., Raftery, P., Schiavon, S., Koupriyanov, M., 2018. Effect of acoustical clouds coverage and air movement on radiant chilled ceiling cooling capacity. Energy Build. 158, 939–949. https://doi.org/10.1016/j.enbuild.2017.10.046

Kuczyński, T., Staszczuk, A., Gortych, M., Stryjski, R., 2021. Effect of thermal mass, night ventilation and window shading on summer thermal comfort of buildings in a temperate climate. Build. Environ. 204, 108126. https://doi.org/10.1016/j.buildenv.2021.108126

Labat, M., Hazyuk, I., 2023. Numerical comparison of an office cooled with and without a ventilated slab using a model predictive controller. Appl. Therm. Eng. 228, 120500. https://doi.org/10.1016/j.applthermaleng.2023.120500

Labat, M., Hazyuk, I., Cezard, M., Lorente, S., 2021. Indoor thermal behaviour of an office equipped with a ventilated slab: a numerical study. J. Build. Perform. Simul. 14, 227–246. https://doi.org/10.1080/19401493.2021.1905714

Labat, M., Virgone, J., David, D., Kuznik, F., 2014. Experimental assessment of a PCM to air heat exchanger storage system for building ventilation application. Appl. Therm. Eng. 66, 375–382. https://doi.org/10.1016/j.applthermaleng.2014.02.025

Lazaro, A., Dolado, P., Marín, J.M., Zalba, B., 2009. PCM–air heat exchangers for free-cooling applications in buildings: Experimental results of two real-scale prototypes. Energy Convers. Manag. 50, 439–443. https://doi.org/10.1016/j.enconman.2008.11.002

Lorente, S., Bejan, A., Niu, J.L., 2014. Phase change heat storage in an enclosure with vertical pipe in the center. Int. J. Heat Mass Transf. 72, 329–335. https://doi.org/10.1016/j.ijheatmasstransfer.2014.01.021

Lu, S., Gao, J., Tong, H., Yin, S., Tang, X., Jiang, X., 2020. Model establishment and operation optimization of the casing PCM radiant floor heating system. Energy 193, 116814. https://doi.org/10.1016/j.energy.2019.116814

Michel, B., Glouannec, P., Fuentes, A., Chauvelon, P., 2017. Experimental and numerical study of insulation walls containing a composite layer of PU-PCM and dedicated to refrigerated vehicle. Appl. Therm. Eng. 116, 382–391. https://doi.org/10.1016/j.applthermaleng.2016.12.117

Mohammad, W.S., Murtadha, T.K., Ahmed, K.A., 2014. Using TermoDeck System for Pre-Cooling/ Heating to Control the Building Inside Conditions. Al-Khwarizmi Eng. J. 10, 13–24.

Mousavi, S., Rismanchi, B., Brey, S., Aye, L., 2024. Operational performance of PCM embedded radiant chilled ceiling using a rule-based control strategy. Energy Build. 310, 114126. https://doi.org/10.1016/j.enbuild.2024.114126

Mousavi, S., Rismanchi, B., Brey, S., Aye, L., 2023. Development and validation of a transient simulation model of a full-scale PCM embedded radiant chilled ceiling. Build. Simul. 16, 813–829. https://doi.org/10.1007/s12273-023-0985-5

Mousavi, S., Rismanchi, B., Brey, S., Aye, L., 2021. PCM embedded radiant chilled ceiling: A state-of-the-art review. Renew. Sustain. Energy Rev. 151, 111601. https://doi.org/10.1016/j.rser.2021.111601

Park, B., Krarti, M., 2019. Optimal control strategies for hollow core ventilated slab systems. J. Build. Eng. 24, 100762. https://doi.org/10.1016/j.jobe.2019.100762

PCM Products Ltd [WWW Document], n.d. URL http://www.pcmproducts.net

Rhee, K.-N., Olesen, B.W., Kim, K.W., 2017. Ten questions about radiant heating and cooling systems. Build. Environ. 112, 367–381. https://doi.org/10.1016/j.buildenv.2016.11.030

Romaní, J., de Gracia, A., Cabeza, L.F., 2016. Simulation and control of thermally activated building systems (TABS). Energy Build. 127, 22–42. https://doi.org/10.1016/j.enbuild.2016.05.057

Royon, L., Karim, L., Bontemps, A., 2014. Optimization of PCM embedded in a floor panel developed for thermal management of the lightweight envelope of buildings. Energy Build. 82, 385–390. https://doi.org/10.1016/j.enbuild.2014.07.012

Rubitherm [WWW Document], n.d. URL https://www.rubitherm.eu/en/index.php/productcategory/makroverkaspelung-csm

Shah, R.K., London, A.L., Engineering, S.U.D. of M., 1971. Laminar Flow Forced Convection Heat Transfer and Flow Friction in Straight and Curved Ducts: a Summary of Analytical Solutions, Technical report. Department of Mechanical Engineering, Stanford University.

Shinoda, J., Kazanci, O.B., Tanabe, S., Olesen, B.W., 2019. A review of the surface heat transfer coefficients of radiant heating and cooling systems. Build. Environ. 159, 106156. https://doi.org/10.1016/j.buildenv.2019.05.034

Soares, N., Costa, J.J., Gaspar, A.R., Santos, P., 2013. Review of passive PCM latent heat thermal energy storage systems towards buildings' energy efficiency. Energy Build. 59, 82–103. https://doi.org/10.1016/j.enbuild.2012.12.042

Stathopoulos, N., El Mankibi, M., Santamouris, M., 2017. Numerical calibration and experimental validation of a PCM-Air heat exchanger model. Appl. Therm. Eng. 114, 1064–1072. https://doi.org/10.1016/j.applthermaleng.2016.12.045

Tarzia, D.A., 2004. An Explicit Solution for a Two-Phase Unidimensional Stefan Problem with a Convective Boundary Condition at the Fixed Face. Conf. Semin. Trab. Mat.

Tittelein, P., Gibout, S., Franquet, E., Johannes, K., Zalewski, L., Kuznik, F., Dumas, J.-P., Lassue, S., Bédécarrats, J.-P., David, D., 2015. Simulation of the thermal and energy behaviour of a composite material containing encapsulated-PCM: Influence of the thermodynamical modelling. Appl. Energy 140, 269–274. https://doi.org/10.1016/j.apenergy.2014.11.055

Voller, V.R., Prakash, C., 1987. A fixed grid numerical mode~~ing methodology for convection-diffusion mushy region phase-change problems. Int. J. Heat Mass Transf. 30, 1709–1719. https://doi.org/10.1016/0017-9310(87)90317-6

Weinläder, H., Körner, W., Strieder, B., 2014. A ventilated cooling ceiling with integrated latent heat storage—Monitoring results. Energy Build. 82, 65–72. https://doi.org/10.1016/j.enbuild.2014.07.013

Weinläder, H., Kranl, D., Strieder, B., 2013. A ventilated cooling ceiling with integrated latent heat storage: test room measurements. Intell. Build. Int. 5, 120–132. https://doi.org/10.1080/17508975.2013.775098

Winwood, R., Benstead, R., Edwards, R., Letherman, K.M., 1994. Building fabric thermal storage: Use of computational fluid dynamics for modelling. Build. Serv. Eng. Res. Technol. 15, 171–178. https://doi.org/10.1177/014362449401500308

Yeo, M.-S., Yang, I.-H., Kim, K.-W., 2003. Historical changes and recent energy saving potential of residential heating in Korea. Energy Build.

Zhuang, Z., Li, Y., Chen, B., Guo, J., 2009. Chinese kang as a domestic heating system in rural northern China—A review. Energy Build. 41, 111–119. https://doi.org/10.1016/j.enbuild.2008.07.013

Zmeureanu, R., Fazio, P., 1988. Thermal performance of a hollow core concrete floor system for passive cooling. Build. Environ. 23, 243–252. https://doi.org/10.1016/0360-1323(88)90009-1

7. Acknowledgments

The authors would like to thank IC Entreprises for supporting this research work and Guillaume Rabut for sharing his experience and expertise related to Vinci's GreenFloor® system. Furthermore, they would like to thank Qianwen Tan, a PhD student at INSA Strasbourg, for her assistance in gathering the information required for the modelling comparison.